GLEX-2021,3,1,8,x62378

Can an airship explore Mars?

Romeo Tonasso[a], Laurène Delsupexhe[b] , Alice Barthe [c]

[a] Master student at Ecole Polytechnique Fédérale de Lausanne, Route Cantonale, 1015 Lausanne, Vaud, Switzerland. Contact: romeo.tonasso@gmail.com
[b] WoMars, chemin des Rupières 3, 1257 Bardonnex, Switzerland. Contact: laurene.delsupexhe@womars.co.uk
[c] WoMars, chemin des Rupières 3, 1257 Bardonnex, Switzerland. Contact: alice.barthe@womars.co.uk

Abstract

The purpose of this study is to assess the conditions and performances of an airship based exploration of Mars. While orbiter based exploration provides global coverage, an airship allows for more proximity to the ground, therefore better spatial resolution as well as better angle of observation of steep relief, such as vertical walls in craters or canyons. This could for instance enable to distinguish geological layers or other small scale geological features. While rover and lander based exploration provide a direct interaction with the surface and very fine analysis, an airship can have a higher ground speed and hover over rough terrains. This gives the possibility to explore large stretches and difficult areas. In fact an airship bridges the gap between orbiter and rover and can be conducted in synergy with them. The scope of this paper is to list the parameters that drive the design, highlight trade-offs and provide a preliminary sizing of the main subsystems. The focus of the study was aerostatic lift based system instead of an aerodynamic lift based system, which shows limitations due for example to the lack of landing facilities. The first part of the study was to gather a state of the art on airships and relevant technologies as well as an estimation of Martian environment's main characteristics. Then, the main drivers for the sizing of the system were identified before proceeding to a preliminary sizing. The Design Reference Mission is to explore parts of Valles Marineris, a 7 km deep canyon in the southern hemisphere of Mars, which was selected for several reasons. Firstly, this region shows interesting geomorphological context with potentially a history of abundance of water. Additionally, the deepness of the canyon yields a higher air pressure. A higher pressure means heavier surrounding air which facilitates the aerostat design. Moreover in the longer run and in a perspective of human presence on Mars, the higher pressure makes this zone more suitable for pressurised habitable installations. The reference scientific goal would be to perform mineral mapping of the cliff walls using a hyperspectral sensor.

Keywords: Airship, Mars, exploration, feasibility, Valles Marineris

Nomenclature

Acronyms

DRM	:	Design Reference Mission
MCD	:	Mars Climate Database
MOLA	:	Mars Orbiter Laser Altimeter
PCE	:	Power Conversion Efficiency

Symbols

a_M	:	Mars' orbit semi-major axis (AU)
am	:	Air mass (/)
A_{CS}	:	Cross-section area (m^2)
A_{sp}	:	Solar panels area (m^2)
Br	:	Beam radiation ($W\,m^{-2}$)
c_D	:	Drag coefficient (/)
D	:	Diameter (m)
e_M	:	Mars' orbital eccentricity (/)
F_D	:	Drag force (N)
F_T	:	Thrust (N)
Ha	:	Hour angle (°)
I_r	:	Received irradiance ($W\,m^{-2}$)
k_T	:	Thrust coefficient (/)
L_s	:	Solar longitude (°)
m	:	Mass (kg)
m_{lift}	:	Liftable mass (kg)
M	:	Molar mass ($kg\,mol^{-1}$)
n	:	Number of (/)
N_{prop}	:	Propeller rotating speed (rev/s)
P_n	:	Necessary propulsive power (W)
P_{sp}	:	Solar panels power (W)
p	:	Static pressure (Pa)
r	:	Radius (m)
r_{SM}	:	Sun-Mars distance (AU)
R_{gas}	:	Universal gas constant ($J\,K^{-1}\,mol^{-1}$)
S_S	:	Solar constant at 1 AU ($W\,m^{-2}$)
t_{env}	:	Envelope thickness (m)
T	:	Temperature (K)
v	:	Flight velocity ($m\,s^{-1}$)
V	:	Volume (m^3)

Greek

γ	:	CO_2 heat capacity ratio (/)
δ	:	Declination angle (°)
δ_0	:	Mars obliquity of rotation axis (°)
η_{ep}	:	Electric propulsion efficiency (/)
η_{sc}	:	Solar cells efficiency (/)
Θ_S	:	True anomaly (°)
θ_S	:	Solar zenith angle (°)
λ_{env}	:	Envelope area density ($kg\,m^{-2}$)
ρ	:	Density ($kg\,m^{-3}$)
σ_t	:	Tangential stress (Pa)
τ	:	Optical depth (/)
ϕ	:	Latitude (°)
ω	:	Propeller rotation speed ($rad\,s^{-1}$)

Subscripts

atm	:	Atmospheric
bal	:	Ballonet
env	:	Envelope
lg	:	Lifting gas
$prop$	:	Propeller

1 Introduction

1.1 Context of the study

The initial project was initiated by the Mars Society Switzerland's president, Pierre Brisson. It resulted in a part time semester project, carried out by Master student Roméo Tonasso, with the regular support of co-authors Laurène Delsupexhe and Alice Barthe.

1.2 Mars exploration systems' state of the art

Firstly, the observation of Mars relies mainly on orbiters, that provide a global coverage of various parameters such as the atmosphere, the geology, or other. Secondly, landers and rovers also have the advantage of directly interacting with the surface of Mars and its regolith. To bridge the gap between the scale of exploration of landers and orbiters, airborne exploration is the perfect candidate, with its ability to go over large stretches of rough terrain, while keeping proximity to the surface. Recently, a step towards airborne exploration of Mars was made thanks to the technology demonstrator Ingenuity and its seven successful flights on the Red Planet.

1.3 A new approach: an airship system

While the aerodynamic system shows promising results, another avenue is aerostatic lift-based system, namely airships. Their usefulness in the context of Mars' exploration was extensively studied by several space agencies (NASA, ROSCOSMOS, CNES) at the end of the millennium (1980s-2000s). More specifically in 2001, NASA's Aerobot Balloon Study (MABS) developed high altitude balloons. The French space agency, CNES, developed a *Montgolfière Infra-Rouge* (MIR), a balloon heated by the sun at an altitude between 20 and 30 km above Earth. All of the systems proposed at the time were "free-floating", meaning no control of their direction and little to none of their altitude was possible. The above is the main heritage to our study, while a growing interest around the use of airship on Earth (e.g. Stratobus by Thales Alenia Space) triggered our will to investigate their use on Mars. Our goal is to revisit the results from this era, in the light of the new materials and technologies available today. In addition, we will investigate what it costs and whether it is possible to go beyond a free floater and actually be able

to stir and control the airship. The scope of this study is limited to the feasibility of such a system, and is not the design of a complete mission. Questions such as fairing, deployment or data processing, as important as they are for an end-to-end mission, are not treated here. The objective is to find the relevant parameters that will drive design, estimate them and accordingly do a first sizing of the main dimensions.

2 Method

The question is not so much whether an airship can fly on Mars, but rather under which conditions and yielding which performances. To answer it, two preliminary steps are necessary: first, estimate the most relevant conditions the airship would face, second, identify the governing equations that will drive the design.

2.1 Atmospheric conditions estimation

Data collected by various rovers and landers during missions such as InSight, Curiosity or Zhurong to name a few, can provide a good overview of the harsh Martian environment. However, the measures are very local in space and time, in the sense that rovers move by tens of kilometers at most and missions sometimes only last a few months. To obtain a more reliable estimation, the Mars Climate Database (MCD) [1, 2] was favoured. It is a tool derived from NASA's Mars General Circulation Model that provide atmospheric information for given coordinates, Martian time, solar longitude and altitude. At most, two parameters can vary. Results are then obtained as a contour plot, for instance function of time and altitude if coordinates and solar longitude are set. Here, the MCD is used to obtain density, pressure and temperature as a function of altitude. The methodology is to arbitrarily chose a number of locations within a zone of interest, then:

- An altitude range is created between the location's depth and the 0 km datum. The increment is variable between locations to have more or less 10 values. (All the altitudes in this study are based on the datum defined by the Mars Orbiter Laser Altimeter (MOLA) aboard the Mars Global Surveyor [3]).
- The solar longitude L_S is also discretized in 0, 90, 180 and 270°.
- L_S is fixed, then an altitude value is fixed and the pressure, temperature and density values as a function of hour are manually retrieved from the MCD.
- The altitude is incremented and once all altitudes have been probed, the L_S is incremented and all altitudes probed again.
- Once all L_S and altitude combinations have been probed, the same is done with the next location.

To treat all these data and obtain evolution with altitude, a Matlab code is used. First, all the values are averaged over a sol, removing the time parameter. The maximum and minimum are also saved. These averages are plotted against altitude for a given location and L_S. A linear approximation is done on the obtained curve, minima and maxima and plotted on the same graph. It was found that temperature is poorly fitted by a linear and square approximation, so a cubic approximation is made. Second, for a similar L_S, the linear approximations of all points are regrouped on the same graph as a function of altitude between -5'000 m and 0 m. Their average is computed as well as the ones of linearized minima and maxima. Considering the non-linear behaviour of temperature in the first thousand meters, only the locations that have a depth close to -5'000 m are used for the lower depths. For upper and lower limits though, all points are taken into account.

2.2 Design Reference Mission

As was explained, defining an operation zone is necessary to select coordinates from which to estimate atmospheric conditions. In addition, it will also impact the solar irradiance computation and mission scenario. A Design Reference Mission (DRM) was hence elaborated in order to define the mission, its operations and its location.

The requirements on the operation zone are multiple. First and foremost, the site presents a geological interest, such as suspected paleohydrology, aqueous minerals, or igneous rocks. In addition, favourable meteorological conditions are necessary for the sustainability of the airship. This includes atmospheric winds (both horizontal and vertical) and surface winds (steady, gusts and sleeping [4]). The most fruitful observations will be in zones of rugged geography such as craters, rifts or canyons. It should be noted that the radius of the landing ellipse has its importance, especially in the case of a canyon that can be uneven. A degree of error is crucial in the difficult operation of landing a vehicle on the Red planet. In terms of simplifying the engineering aspect, the zones to favour are firstly close to the equator, as they offer better weather conditions, and secondly at the lowest altitude possible, to obtain a maximal atmospheric density. The Hellas impact basin was considered, as it features the deepest point on Mars at -8'200 m and has a mean depth around -7'000 m, but its mission interest is limited. An interesting region is Valles Marineris, an aggregate of canyons more than 4'000 km long and 200 km wide. It is situated in the southern hemisphere close, and rather parallel, to the equator, at a mean latitude about 10°S. Within Valles Marineris, Melas Chasma is the widest segment of the canyon system. Its eastern and south-western part, shown on figure

1 below, were studied in more details.

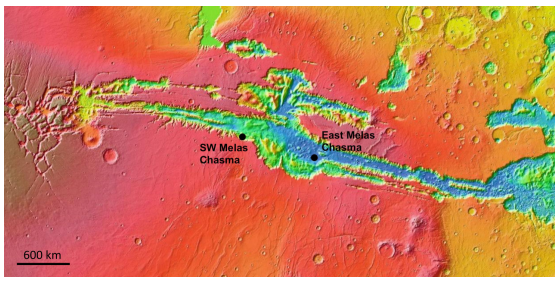

Figure 1: Valles Marineris - Eastern and south-western Melas Chasma (from Mars Global Surveyor, image credit: NASA/JPL-Caltech/Arizona State University)

For the eastern location, the MCD revealed that there were no vertical winds - either surface (figure 2) or atmospheric (figure 7 in appendix A), throughout the day or year and that the surface winds' velocity peaked at 9 m/s, with an average velocity of 3.5 m/s. In addition, satellite pictures revealed fluvial material and potentially aqueous minerals, with a high albedo - which implies the surface is lighter and therefore reflects the solar rays, increasing the irradiance. As for the south-western of Melas Chasma, it was in fact amongst the eight finalists for Perseverance's landing sites. In terms of the topography, its main interest is its large paleolake. Its radius fits the landing ellipse requirement and the center of the landing ellipse is situated at a depth of -1'920 m. Surface winds (figure 8 in appendix A) are lower than those of the eastern location, with a peak at 6.5 m/s. However, atmospheric winds (figure 9 in appendix A) had a slightly higher peak at 11 m/s and an average of 7 m/s throughout the day. The geology presents debris material from canyon walls as old as 200-300 millions of years, as well as a many fluvial and subaqueous features like deltas or lacustrine deposits. The scientific potential of this site proved to be extensive. As both sites are of interest and relatively close, the operation zone (shown in figure 3) is defined to be in a latitude between 8°S and 13°S, and longitude between 80°W and 65°W. The altitudes where the airship will operate are obviously only the negative ones.

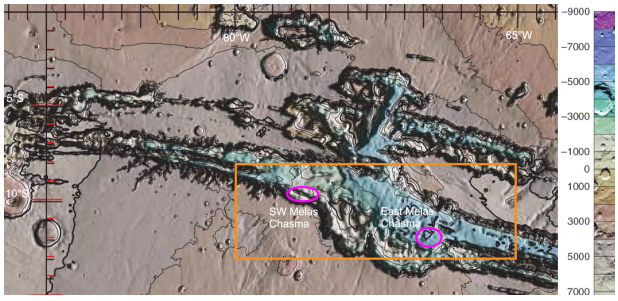

Figure 3: Operation zone (orange) in Valles Marineris (Color-Coded Contour Map of Mars by U.S. Geological Survey)

2.3 *Local conditions*

With the DRM defined, five geographic points are taken. They are arbitrarily chosen in the operation zone of the airship. With them, and following the approach previously described in section 2.1, the obtained estimations of pressure, temperature and density are compared for different L_S. Figure 4 shows the most favourable season is for a solar longitude of 90° (southern winter beginning), as it has the highest atmospheric density. Corresponding graphs of pressure and temperature graphs are shown in figure 10 in appendix B.

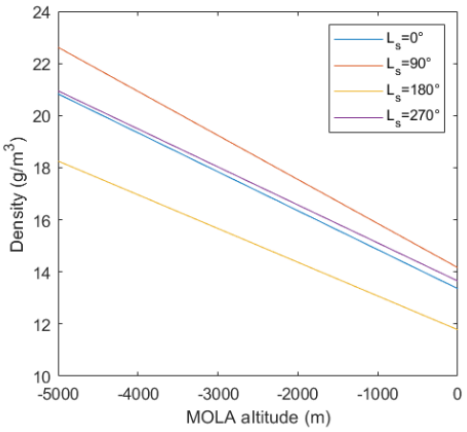

Figure 4: Mean atmospheric density with altitude

With the operation zone defined, solar irradiance can also be found. It is estimated in two ways: with the theoretical equation (detailed later) and again with the MCD for confirmation.

2.4 *Thrust coefficient estimation*

As explained further later, the Martian atmosphere makes propeller-generated thrust quite challenging. One of the key elements is the thrust coefficient, that depends on the propeller's design. References of Mars intended propellers are rather scarce compared to Earth ones, luckily Ingenuity recently performed successful flights. The thrust coefficient is thus estimated based on its scaling (dimensions in table 1).

Parameter	Value	Unit
Rotor speed N	2'400	rpm
Propeller diameter D_{prop}	1.2	m
Number of propellers n_{prop}	2	/
Mass m	1.8	kg

Table 1: Ingenuity's main dimensions

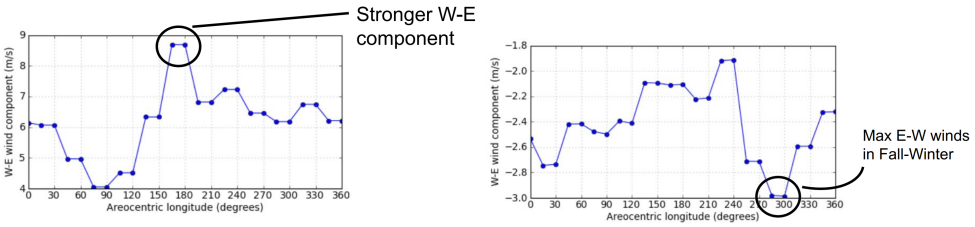

Figure 2: Eastern Mellas Chasma - Surface winds 10 m above surface (from MCD)

3 Theory and calculations

The three main subsystems of the airship are investigated: its envelope, its power and its propulsion. The aim is to identify the equations relevant to establish feasibility.

3.1 Envelope

3.1.1 Envelope sizing

The envelope's design is the key features of the airship. It is chosen to have a closed envelope containing hydrogen as lifting gas. Indeed, it could be obtained on Mars with electrolysis and is not subject to flammable hazards thanks to the absence of oxygen. The lifting gas is never vented, as it implies refilling which would complicate operation beyond reason. Assumptions are that both the atmosphere and lifting gas follow the ideal gas law and that the lifting gas is at atmospheric temperature. For the envelope to maintain its shape, it is also decided to have a lifting gas pressure 1.5 times the outside one. The mass liftable by the envelope in kilograms m_{lift}, with the envelope mass already accounted for, is given by:

$$m_{lift} = (\rho_{atm} - \rho_{lg}) \cdot V_{lg} - m_{env} \quad (1)$$

With:
- ρ_{atm} the atmospheric density (kg m^{-3})
- ρ_{lg} the lifting gas density (kg m^{-3})
- V_{lg} the lifting gas' volume (m^3)
- m_{env} the envelope's mass (kg)

The lifting gas' density is computed with the ideal gas law and assumptions made:

$$\rho_{lg} = \frac{p_{lg} M_{lg}}{R_{gas} T_{lg}} = 1.5 \frac{p_{atm} M_{lg}}{R_{gas} T_{atm}} \quad (2)$$

With:
- p_{atm} the atmospheric pressure (Pa)
- M_{lg} the molar mass of lifting gas ($2.016 \cdot 10^{-3}$ kg mol^{-1} for hydrogen)
- R_{gas} the universal gas constant (8.314 J K^{-1} mol^{-1})
- T_{atm} the atmospheric temperature (K)

On Earth, airships have an aerodynamic profile to minimise drag. A quick order of magnitude comparison of dynamic pressure with density values of respectively 0.02 kg m^{-3} and 1.2 kg m^{-3} shows that the Martian wind has to be close to eight times faster on Mars to achieve a similar dynamic pressure. Optimising the envelope's profile is not a priority on Mars, a spherical envelope shape is hence chosen, as it has the best volume to surface ratio or in other words, the lowest envelope mass for a given volume. For a sphere, equation 1 becomes:

$$m_{lift} = \frac{4\pi}{3}(\rho_{atm} - \rho_{lg}) \cdot r_{env}^3 - 4\pi\lambda_{env} \cdot r_{env}^2 \quad (3)$$

With:
- r_{env} the radius of the envelope (m)
- λ_{env} the envelope's surfacic density (kg m^{-2}).

As expected, the envelope's material needs to be as lightweight as possible.

3.1.2 Envelope material

Mylar[1] is the preferred material for balloons and airships due to its extremely low permeability but it has two main disadvantages. Not only is its tear resistance low, making holes and imperfections likely to propagate, but it also is UV sensitive. It is estimated that the tensile strength is reduced by 30% after 120h of Mars UV exposure [5]. It is thus best for the airship envelope to be a composite. At least three layers are needed, from inside to outside: a gas retention layer, a load bearing layer and an outside protection layer, with the whole bounded by adhesive layers in between. An example of such composite is from the NASA Balloon Program [6] that uses 3.5 μm of Mylar, a scrim of Kevlar 55 denier and 6 μm of polyethylene as outside protection with adhesive layers between each. Having Kevlar in scrim form allows to limit the added weight. The obtained total surfacic mass is 19.66 g/m^2 but neither the exact thickness of the scrim, nor the yield strength are stated. Other similar composition examples were found with Mylar ranging from 3.5 to 12 μm.

[1] commercial name of BoPET (Biaxially-oriented Polyethylene Terephthalate)

Vasudevan et al [7] made a comparative of materials for a three layer composite aimed at a high altitude helium airship. Their conclusion is the following:

- Gas retention layer: Mylar, a polyester based film, for its low permeability, high strength, dimensional stability and flex fatigue resistance.
- Load bearing layer: Vectran, a polyester based woven fabric, for its minimum elongation, high tear resistance and dimensional stability.
- Outer protection layer: Tedlar, a polyvinyl fluoride (PVF), for its excellent resistance to weathering and chemicals. PVF also has a fair resistance to UV exposure and a low permeability.
- Adhesive: Hytrel, a polyester based elastomer, for its strong adhesion capabilities and enhancement of impermeability.

Earth's high altitude atmosphere shows similarities with Mars' atmosphere, so this configuration fits the present use. However, the thickness they use for the first two layers is 200 μm while the third is 1mm. Compared to other values gathered from the studies mentioned, this seems excessively high for a Martian application, especially regarding the third layer. Indeed, their study uses helium as lifting gas, which is monoatomic whereas hydrogen is diatomic, we can hence hope for a better retention. Additionally, high altitude airships on Earth are usually designed to float for months without landing and face harsher weather conditions. The thickness of all layers is therefore scaled down based on other values found in studies mentionned. The corresponding surfacic density are computed from the densities given in [7].

Layer	Thickness	Area density
Mylar	6 μm	16.7 g/m^2
Vectran	12 μm	16.8 g/m^2
Tedlar	6 μm	9.27 g/m^2
Total	24 μm	42.77 g/m^2

Table 2: Envelope materials mass and thickness breakdown

The obtained area density is more than twice that of the NASA Balloon Program. It is probably possible to have a lighter envelope but this value is kept not to have a too optimistic scenario.

As the envelope's thickness will be several orders of magnitude smaller than its radius, is a thin walled sphere. The stress in the material is thus expressed as:

$$\sigma_t = \frac{r_{env}\Delta p}{2t_{env}} \tag{4}$$

With:
- σ_t tangential stress (Pa)
- Δp the pressure difference between inside and outside (Pa), in our case 0.5 p_{atm}
- t_{env} the thickness of the envelope (m)

There are three possibilities for the envelope design: having a constant pressure, a constant volume or using inner balloons (also called ballonets). For temperature changes between 180 K and 260 K (extremes found for L_S=270°), maintaining the pressure constant would mean that the volume ratio between hottest and coldest temperature is:

$$\frac{V_{lg}^{max}}{V_{lg}^{min}} = \frac{T_{lg}^{max}}{T_{lg}^{min}} = \frac{260}{180} = 1.44 \tag{5}$$

An 44% volume increase appears too challenging in terms of materials, constant pressure is therefore rejected. Maintaining a constant volume would mean an additional altitude control mean is needed so ballonets are the preferred solution if altitude control is essential.

3.1.3 Ballonet sizing

When the ballonet is filled with ambient gas, it reduces the lifting gas volume and increases the mass carried, so the airship goes down. Its size ensues from the wanted altitude range: the same mass has to be lifted at the lowest altitude, where the ballonet is fully inflated, as at the highest altitude, where it is fully deflated. It is assumed that there is a single spherical ballonet, at equal pressure and temperature with the envelope's content in steady state. Again, the simplifying assumption that the ambient gas is ideal is made. Equation 1 becomes:

$$m_{lift} = (\rho_{atm} - \rho_{lg}) \cdot V_{lg} - \lambda_{env} S_{env} - m_{bal} \tag{6}$$

Where m_{bal} is the ballonet's mass (kg), neglecting its envelope and only considering its content for now. With the previous assumptions we have:

$$m_{bal} = p_{bal} \frac{V_{bal} M_{bal}}{R_{gas} T_{bal}} \tag{7}$$

$$m_{bal} = 1.5 \cdot p_{atm} \frac{V_{bal} M_{atm}}{R_{gas} T_{atm}} \tag{8}$$

$$m_{ba} = 1.5 \cdot \rho_{atm} V_{bal} \tag{9}$$

With:
- p_{bal} the pressure in the ballonet (Pa)
- V_{bal} the ballonet's volume (m^3)
- M_{bal} the molar mass of the ballonet's content (kg mol^{-1})
- T_{bal} the temperature of the ballonet's content (K)

To lift the same mass at a minimum altitude h_0 and a maximum altitude H:

$$[(\rho_{atm} - \rho_{lg}) \cdot V_{lg}]_{h_0} - \lambda_{env} S_{env} - 1.5 \ ...$$

$$\cdot \rho_{atm}|_{h_0} V_{bal} = [(\rho_{atm} - \rho_{lg}) \cdot V_{lg}]_H - \lambda_{env} S_{env} \quad (10)$$

The $\lambda_{env} S_{env}$ term is constant, so it cancels on each side. $V_{lg}|_H$ is renamed as V_{env} for simplicity, since it is the complete envelope's volume (empty ballonet).

$$[\rho_{atm} V_{lg}]_{h_0} - [\rho_{lg} V_{lg}]_{h_0} - 1.5 \cdot \rho_{atm}|_{h_0} V_{bal} \ ...$$

$$= \rho_{atm}|_H V_{env} - \rho_{lg}|_H V_{env} \quad (11)$$

The $[\rho_{lg} V_{lg}]_{h_0}$ term on the left and $\rho_{lg}|_H V_{env}$ term on the right both are the total mass of lifting gas, which is constant. Also using the fact that $V_{lg}|_{h_0} = V_{env} - V_{bal}$ we get:

$$\rho_{atm}|_{h_0} V_{env} - \rho_{atm}|_{h_0} V_{bal} - 1.5 \cdot \rho_{atm}|_{h_0} V_{bal} \ ...$$

$$= \rho_{atm}|_H V_{env} \quad (12)$$

Using $\Delta\rho$ for the density amplitude $\rho_{atm}|_{h_0} - \rho_{atm}|_H$, the volume of the ballonet is defined by:

$$V_{bal} = \frac{\Delta\rho_{atm} V_{env}}{2.5 \rho_{atm}|_{h_0}} \quad (13)$$

3.2 Power

3.2.1 Necessary propulsive power

To have a steady flight, the airship has to overcome the drag force. Based on the wind values found in the DRM, a velocity of 10 m s^{-1} is selected. Dynamic viscosity can be estimated using Sutherland's law (equation 14), which approximates dynamic viscosity of single component gases at low pressure. CO_2 accounting for more than 95% of the Martian atmosphere it can reliably be used.

$$\mu = \mu_0 \left(\frac{T}{T_0} \right)^{\frac{3}{2}} \frac{T_0 + S}{T + S} \quad (14)$$

With:
- μ_0 is the reference viscosity ($Pa \cdot s$) at the reference temperature T_0 (K)
- S Sutherland's constant (K), which is 222 K for CO_2 in the 190-1'700 K range with a 2% error [8].

With this known, and the envelope's radius fixed, the Reynolds number can be computed. Doing so allows to estimate the drag coefficient c_D of the airship, which in turn yields the drag force F_D and necessary power P_n:

$$P_n = F_D \cdot v \quad (15)$$

[2]Unless indicated otherwise numerical values are from [9]

$$P_n = \frac{1}{2} \rho_{atm} v^2 A_{CS} \ c_D \cdot v \quad (16)$$

Where A_{CS} is the cross-section area of the airship (m^2), so:

$$P_n = \frac{1}{2} \rho_{atm} v^3 \pi r_{env}^2 c_D \quad (17)$$

3.2.2 Available solar power

Solar irradiance is dependant on three factors: the Sun-Mars distance, the solar zenith angle θ_S and atmospheric attenuation. The solar radiation reaching the top of Mars' atmosphere, or beam radiation, can be expressed as:

$$Br = \frac{S_S}{r_{SM}^2} \quad (18)$$

With:
- S_S the solar constant[2] at 1 AU (1'361 W m^{-2})
- r_{SM} the Sun-Mars distance (AU)

Given Mars' elliptical orbit, that distance varies during the year and can be in turn expressed as:

$$r_{SM} = \frac{a_M (1 - e_M^2)}{1 + e_M \ cos(\Theta)} \quad (19)$$

With:
- a_M Mars' orbit semi major axis in AU (1.524 AU)
- e_M the orbital eccentricity (0.0935)
- $\Theta = L_s - 248°$ the true anomaly (°)

With this, equation 18 becomes:

$$Br = \frac{S_S (1 + e_M \ cos(L_s - 248))^2}{a_M^2 (1 - e_M^2)^2} \quad (20)$$

During the day, the solar zenith angle will go from 90° to 0° back to 90°. Its cosine can be expressed as a function of time with the equation:

$$cos(\theta_S) = sin\delta \ sin\phi + cos\delta \ cos\phi \ cos(Ha(t)) \quad (21)$$

With:
- δ the declination angle (°): the angular position of the Sun at noon with respect to the equatorial plane. Its range is thus determined by the planet's obliquity as $sin\delta = sin\delta_0 \ sin(L_s)$ (from [10]), where $\delta_0 = 25.19°$ is the Mars obliquity of rotation axis.
- ϕ the latitude (°)
- $Ha(t)$ the hour angle (°): a conversion of local solar time in degrees. It is 0 at solar noon, negative before noon and positive after noon. From now on, Martian hours will be used instead of regular hours for convenience: a 24.6597 hours sol is thus considered 24 Martian hours. This means that a one hour angle is 15°, hence $Ha(t) = 15 \cdot t - 180$.

The last factor to take into account is the atmosphere. Irradiance has three components: direct, diffuse and reflected irradiance. For simplicity we only consider direct irradiance, which is an underestimation. The attenuation of the beam radiation received at the top of the atmosphere is given by Beer's law:

$$I_r = Br \cdot exp(-\tau \cdot am(\theta_S)) \tag{22}$$

With:
- I_r the received irradiance (W m^{-2})
- τ the optical depth (/)
- $am(\theta_S)$ the air mass (/), the optical path ratio between θ_S and $\theta_S = 0 = \frac{1}{cos(\theta_S)}$ (from [10])

The received irradiance is therefore:

$$I_r = \frac{S_S(1 + e_M\ cos(L_s - 248))^2}{a_M^2(1 - e_M^2)^2} \cdot exp\left(\frac{-\tau}{cos(\theta_S)}\right) \tag{23}$$

with $cos(\theta_S)$ expressed in equation 21.

For the latitude range considered, the irradiance received outside of the 7-17h windows is either negligible or null. The energy received per sol is thus computed for all solar longitudes by increments of 10° by integrating the irradiance between 7 and 17h, Martian hours. An optical depth of 0.4 is chosen based on [10] and [11], according to which τ=0.1 is a clear sky and τ=2 a large dust storm. The result if visible in figure 5. Southern autumn (L_S between 0° and 90°) is the least favourable period, while the southern spring (L_S between 180° and 270°) is the most favourable. L_S=90° was the best period in terms of density[3] so a trade-off has to be made between a higher irradiance, meaning less solar panels mass so a smaller envelope, and a higher density, also meaning a smaller envelope size.

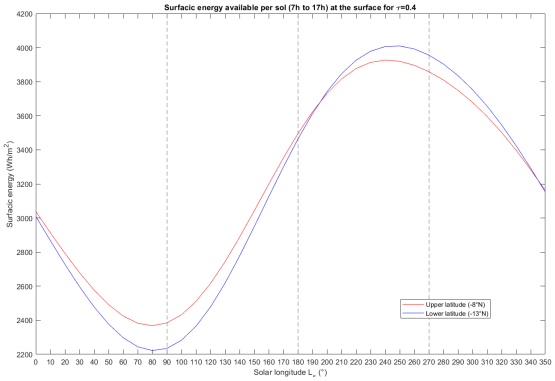

Figure 5: Computed available surfacic energy

The two solar longitude possibilities were compared and the difference in envelope radius turned out to be negligible compared to its overall size. A solar longitude of 270° (southern summer beginning) is hence selected as it will reduce the necessary solar panels surface, making their integration to the airship easier. The estimated irradiance during a sol is thus the one shown in figure 6.

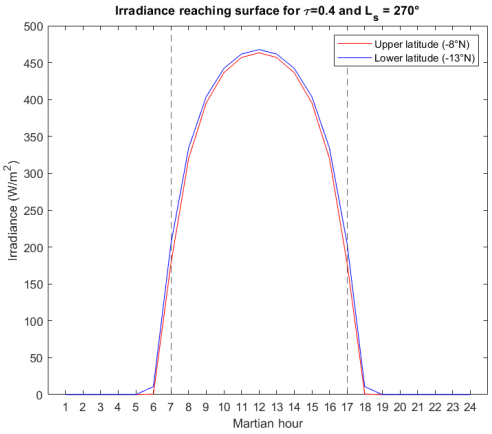

Figure 6: Estimated irradiance over a sol at summer solstice

To assess the exactness of the results, the Mars Climate Database is used at a latitude of 10°S with an average solar scenario (appendix C). It shows that the theoretical estimation underestimates the received irradiance during the peak hours from 10 to 14h up to 23%, in part due to the optical depth selected. The estimated irradiance is still kept as a worse case.

3.2.3 Power production

To generate the necessary power, solar panels are the favoured solution. Multijunction solar cells use several layers of semiconductor materials to absorb different ranges of the wavelength spectrum and thus increase efficiency. In particular, triple junction (3J) inverted metamorphic multijunction (IMM) cells use a germanium (Ge) or Gallium Arsenide (GaAs) base with additional layers usually derived from gallium, such as indium gallium arsenide (InGaAs) or indium gallium phosphide (InGaP) to reach Power Conversion Efficiencies (PCE) above 30%. Table 3 below shows the specifications of some IMM 3J cells, except for the spectrolab ones that are just 3J.

[3] It is important to note that this is not necessarily the optimum, solar longitude was discretized by coarse increments of 90° when retrieving atmospheric data from the MCD, as it is a lengthy process, so the optimum might be at 240° for example.

Reference	Max. PCE (BOL)	Cells thickness	Area density
Microlink Devices [12]	$> 30\%$	$< 50\mu$m	< 250 g/m^2
Spectrolab [13]	30.5%	80-225 μm	500-840 g/m^2
JAXA [14]	32%	$> 20\mu$m	/
"3J-IMM Solar Cell"[15]	32.4%	23 μm	120 g/m^2

Table 3: Solar cells comparison

In light of this, conservative values of 50 μm thickness, 200 g/m^2 surfacic density and 25% PCE are chosen for the rest of the study. To obtain a complete array, cells have to be fixed to a conductive substrate material, coated, then the whole bounded together. A reference of IMM panels intended for Martian ground [16] is taken for masses and thicknesses other than the cells.

Layer	Thickness	Area density
Protective layer	80 μm	90 g/m^2
Coating	/	1.5 g/m^2
Solar cells	50 μm	200 g/m^2
Conductive layer	1 μm	4.5 g/m^2
Substrate	200 μm	129 g/m^2
Total	331 μm	425 g/m^2

Table 4: Solar panel's mass and thickness breakdown

The power generated by the solar panels is found with:

$$P_{sp} = \eta_{sc} I_r A_{sp} \tag{24}$$

With:
- P_{sp} the power produced by solar panels (W)
- η_{sc} the PCE of the cells (/)
- A_{sp} the area of solar panels (m^2)

Solar panels will provide the necessary energy between 7h and 17h, so batteries will be necessary for the remaining hours. Two choices are possible: the first is to have a minimal amount of batteries to only power communications and the on-board computer, in which case the airship would have to land or anchor itself. The second is to have a much larger amount of batteries to retain propulsion and altitude control abilities. One strategy is not recommended over the other here, but batteries are sized for the latter case to provide an idea of the orders of magnitude at stake in the worst case. Sizing is done in the following way:
As a worst case, it is assumed that the airship operates continuously at 10 m/s. A power budget is made that subtracts the necessary power to the produced power. Depending on the time of day, the budget is positive or negative. The deficit is integrated over hours where the budget is negative to find the total energy deficit. Dividing it by the energy density of batteries gives the corresponding necessary mass of batteries, also taking the depth of discharge into consideration. It is also checked that the power exceeding is sufficient to recharge the batteries during day hours.

3.3 Propulsion sizing

The propulsion strategy is to use propellers. To generate the necessary power, the necessary thrust is:

$$F_T = \frac{\eta_{ep} P_n}{v} \tag{25}$$

Where η_{ep} is the overall electric propulsion efficiency found with table 5.

Component	Efficiency
Electronics	0.98
Motor efficiency	0.9
Gearbox efficiency	0.85
Propeller efficiency	0.85
Overall efficiency	0.637

Table 5: Electric propulsion efficiency (values from [17])

The thrust generated by a single propeller can be expressed as:

$$F_T = k_t \rho_{atm} N_{prop}^2 D_{prop}^4 \tag{26}$$

With:
- k_t the thrust coefficient (/)
- N_{prop} the rotating speed (rev/s)
- D_{prop} the propeller diameter (m)

The constraints on the propeller are that it shall provide at least the necessary thrust and that its tip remains subsonic, that is:

$$\omega \frac{D_{prop}}{2} < f_s \cdot \sqrt{\gamma \frac{R_{gas}}{M_{atm}} T_{atm}} \tag{27}$$

With:
- ω the propeller's rotation speed (rad s^{-1})
- f_s a safety factor (< 1)
- γ the atmosphere's heat capacity ratio (/), approximated as CO_2 (about 1.28)
- M_{atm} the atmosphere's molar mass (kg mol^{-1})

Equations 26 and 27 define a lower and upper limit for the diameter and velocity combination.

As mentioned in the method part, Ingenuity's two propellers generate enough thrust to compensate the helicopter's weight, which allows to deduce the thrust coefficient value for propellers on Mars.

4 Results

With all the necessary equations described, the parameters just have to be inserted.

4.1 Envelope

As a starting point, a liftable mass of 500 kg is assumed, with the envelope's own mass already compensated. An altitude range between -5'000 m and -2'000 m is selected. For L_S = 270°, the mean atmospheric density, pressure and temperature at that altitude are found to be 0.01657 kg m^{-3}, 721 Pa and 231 K, with the profile established with the MCD. With these inputs, the envelope area density given in table 2 and equation 2, equation 3 yields a radius of 22.97 m when solved numerically. With the radius, envelope thickness and atmospheric pressure at -5'000 m, the maximum envelope stress is found to be 216 MPa. As a reference, Vectran has a tensile strength of 565 MPa. Using equation 13, the ballonet needs a radius of 10 m.

4.2 Power

With the envelope diameter, airship velocity and a $1.18{\cdot}10^{-5}$ Pa·s dynamic viscosity, the Reynolds number is $6.44{\cdot}10^{5}$. This is just around the drag crisis of a smooth sphere, so a rather low drag coefficient of 0.2 is selected. This results in a necessary power of 2'746 W. With 0.25 PCE cells and the irradiance profile found for L_S=270°, the necessary solar panels area is 29 m^2. Their total mass is 12.34 kg, based on table 4's values. With a 400 Wh/kg energy density and an 80% depth of discharge, the batteries mass is 111.57 kg.

4.3 Propulsion

Finally, for the propulsion, the necessary thrust is 175 N. If two propellers are used, their optimal diameter and rotation speed are 4.12 m and 991 rpm. If four propellers are used instead of two, the optimum is a 2.91 m diameter at 1'400 rpm.

4.4 Mass budget

A mass budget is performed to evaluate the remaining margin out of the initial 500 kg liftable mass.

Component	Mass (kg)
Batteries	111.57
Ballonet's envelope	25.33
Propulsion	26.75
Solar panels	12.34
Instrument	3
Total	179
Margin	321

Table 6: Mass budget

The ballonet's envelope is assumed to be Mylar only. Propulsion is comprised of motors, controller, gearbox and propellers. The first three are estimated with scaling factors of 1'291 W/kg, 6'233 W/kg and 3'279 W/kg respectively (from [18]). The propeller's weight is an upscale of a known 10 kg, 3.5 m diameter propeller. Finally, the instrument is assumed to be a hyperspectral camera. Out of the initial 500 kg payload, 321 kg remain for the gondola's structure, telecommunications, on-board computer, and such.

5 Discussion

Some aspects have not yet been studied here and would help refine the feasibility conditions. It is the case of the mass and power budget associated to the ballonet or hydrogen retention, that will likely be the limiting factor of the mission duration. Nevertheless, the governing sizing parameters of an airship have been found. As was expected from the start, a large envelope is necessary, which impacts all the sizing. On Earth that is not problematic, but on Mars it means complex folding of the envelope and propellers, first to accommodate it in the restricted volume of a fairing and second to deploy it without damage. Here, the focus was on the physical laws applying on site, the next step would be to study the airship's architecture: arranging the propellers and solar panels on the gondola will be no easy task. In particular, considering the envelope's size, the panels risk to be in its shadow. The alternative would be to integrate the cells directly to the top of the envelope but this will affect the envelope's flexibility, create interface issues, and result in a non-homogeneous material. A potential solution would be to have a semi-rigid airship, with parts of the envelope more rigid than the rest, to spread the weight force. A "belt" in a longitudinal way would allow to attach the gondola at the bottom, propellers on the side and solar panels on the top. Alternatively, the envelope's structural resistance could be improved in other ways, for instance with a pumpkin shape or internal tethers to constrain it. In any case, the interface between the envelope and the gondola, or any rigid component, will be a sensitive region.

6 Conclusion

This study concludes that it is physically possible to fly and control an airship on Mars, with relevant scientific outcomes. Dimensions for the most important aspects of the airship were found, yet numerical results are not the primary goal here. Indeed, it is the conditions and governing equations driving the design that are the core aspect. Technologies will improve but physical laws will remain the same, so linking these equations with an Excel file or any type of code allows to easily change the input parameters to adapt to different scenarios, materials and technologies. It is hoped that this study has helped in updating the concept of an aerostat on the red planet and will allow further deeper studies.

Acknowledgements

We would like to thank Mr. Pierre Brisson, president of the Mars Society Switzerland, and Mr. Claude Nicollier, honorary Professor at the Ecole Polytechnique Fédérale de Lausanne and former ESA astronaut, for their tremendous help and precious advice during this project. In addition, we are grateful for Mrs. Julie Hartz's input on the geological aspect of the Design Reference Mission.

Appendices

A Mellas Chasma wind plots

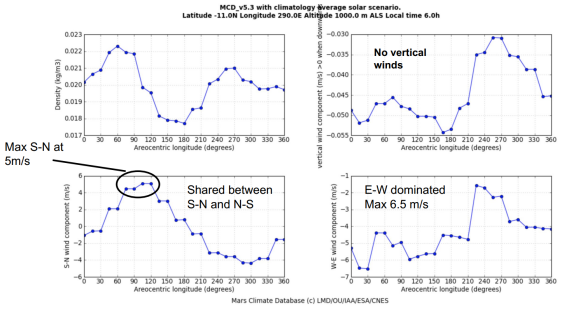

Figure 7: Eastern Mellas Chasma, 1'000 m above the surface - Atmospheric winds (from MCD)

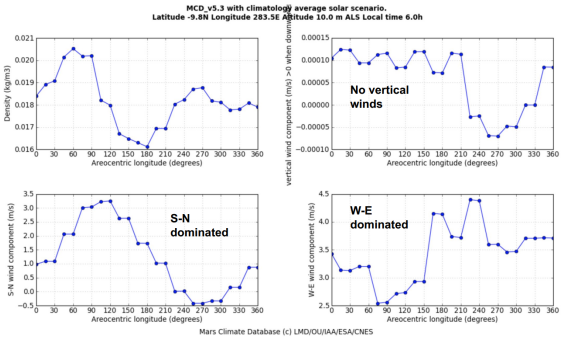

Figure 8: South Western Mellas Chasma, 10 m above the surface - Surface winds (from MCD)

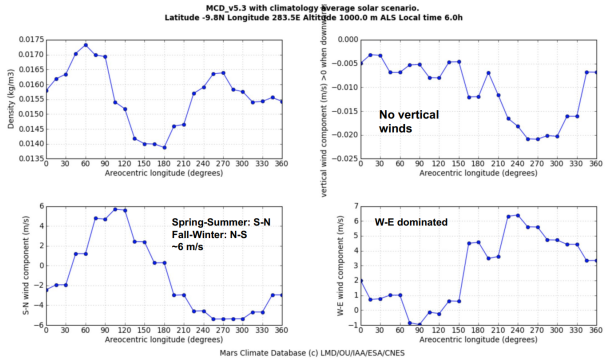

Figure 9: South Western Mellas Chasma, 1'000 m above the surface - Atmospheric winds (from MCD)

B Estimation of the atmospheric conditions in Melas Chasma

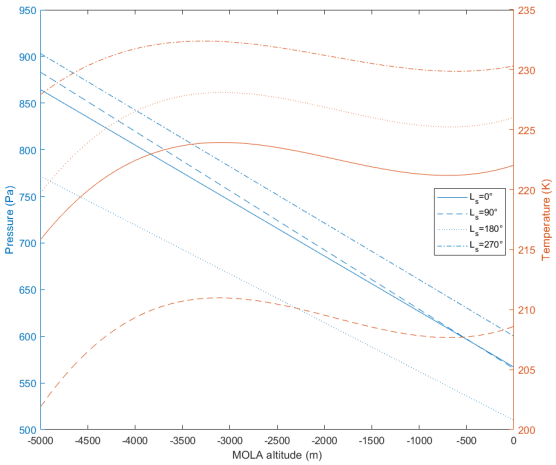

Figure 10: Mean atmospheric pressure and temperature with altitude

C Solar irradiance assessment with MCD

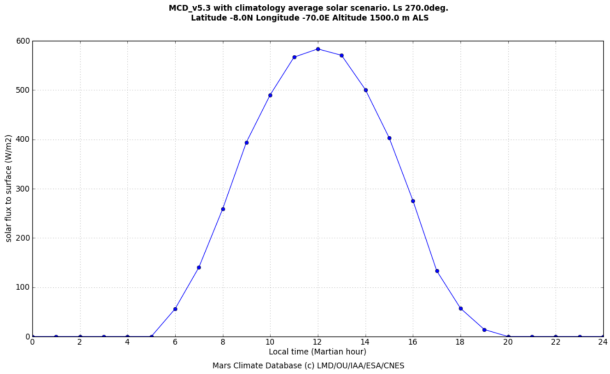

Figure 11: Irradiance over a sol from MCD

References

[1] E. Millour et al. “The Mars Climate Database (version 4.3)”. In: International Conference On Environmental Systems. July 12, 2009, pp. 2009–01–2395. doi: 10.4271/2009-01-2395. url: https://www.sae.org/content/2009-01-2395/.

[2] François Forget et al. “Improved general circulation models of the Martian atmosphere from the surface to above 80 km”. In: 104.E10 (Oct. 1999), pp. 24155–24176. doi: 10.1029/1999JE001025.

[3] *MOLA PRECISION EXPERIMENT DATA RECORD (PDS)*. url: https://nssdc.gsfc.nasa.gov/nmc/dataset/display.action?id=PSPG-00856.

[4] John A. Grant et al. “The science process for selecting the landing site for the 2020 Mars rover”. In: *Planetary and Space Science* 164 (Dec. 1, 2018), pp. 106–126. issn: 0032-0633. doi: 10.1016/j.pss.2018.07.001. url: https://www.sciencedirect.com/science/article/pii/S0032063318301077.

[5] Andre Girerd and Andre Girerd. “A case for a robotic Martian airship”. In: *12th Lighter-Than-Air Systems Technology Conference*. 12th Lighter-Than-Air Systems Technology Conference. San Francisco,CA,U.S.A.: American Institute of Aeronautics and Astronautics, June 3, 1997. doi: 10.2514/6.1997-1460. url: http://arc.aiaa.org/doi/10.2514/6.1997-1460.

[6] Terry Gamber et al. “Mars 2001 Aerobot/Balloon System overview”. In: *International Balloon Technology Conference*. International Balloon Technology Conference. San Francisco,CA,U.S.A.: American Institute of Aeronautics and Astronautics, June 3, 1997. doi: 10.2514/6.1997-1447. url: http://arc.aiaa.org/doi/10.2514/6.1997-1447.

[7] Durga Vasudevan et al. “Analysis and retardation of helium permeation for high altitude airship envelope material”. In: 1ST INTERNATIONAL CONFERENCE ON ADVANCES IN MECHANICAL ENGINEERING AND NANOTECHNOLOGY (ICAMEN 2019). Jaipur, India, 2019, p. 030027. doi: 10.1063/1.5123949. url: http://aip.scitation.org/doi/abs/10.1063/1.5123949.

[8] Frank M. White. *Viscous Fluid flow*. Second edition. 1991. url: http://servidor.demec.ufpr.br/CFD/bibliografia/viscous_fluid_flow_frank_m_white_second_edition.pdf.

[9] *Mars Fact Sheet*. url: https://nssdc.gsfc.nasa.gov/planetary/factsheet/marsfact.html.

[10] Joseph Appelbaum and Dennis J. Flood. “Solar radiation on Mars”. In: *Solar Energy* 45.6 (1990), pp. 353–363. issn: 0038092X. doi: 10.1016/0038-092X(90)90156-7. url: https://linkinghub.elsevier.com/retrieve/pii/0038092X90901567.

[11] Joel S. Levine, David R. Kraemer, and William R. Kuhn. “Solar radiation incident on Mars and the outer planets: Latitudinal, seasonal, and atmospheric effects”. In: *Icarus* 31.1 (May 1, 1977), pp. 136–145. issn: 0019-1035. doi: 10.1016/0019-1035(77)90076-8. url: http://www.sciencedirect.com/science/article/pii/0019103577900768.

[12] Microlink Devices Inc. *MicroLink_Devices_212.pdf*. url: https://www.arpae-summit.com/paperclip/exhibitor_docs/14AE/MicroLink_Devices_212.pdf.

[13] Spectrolab. *XTJ-Prime_Data_Sheet.pdf*. url: https://www.spectrolab.com/photovoltaics/XTJ-Prime_Data_Sheet.pdf.

[14] Mitsuru Imaizumi et al. “QUALIFICATION TEST RESULTS OF IMM TRIPLE-JUNCTION SOLAR CELLS, SPACE SOLAR SHEETS, AND LIGHTWEIGHT&COMPACT SOLAR PADDLE”. In: (2017), p. 6.

[15] A. B. Cornfeld and J. Diaz. “The 3J-IMM solar cell: Pathways for insertion into space power systems”. In: *2009 34th IEEE Photovoltaic Specialists Conference (PVSC)*. 2009 34th IEEE Photovoltaic Specialists Conference (PVSC). ISSN: 0160-8371. June 2009, pp. 000954–000959. doi: 10.1109/PVSC.2009.5411129.

[16] Gabrielle S. Adams et al. *Utilization of Solar Cell Umbrellas to Provide Long- Term Photovoltaic Power on Mars*. 2018. url: http://bigidea.nianet.org/wp-content/uploads/2018/03/2018-BIG-Idea-Final-Paper_TAMU-1.pdf.

[17] Anthony J Colozza, Analex Corporation, and Brook Park. “Comparison of Mars Aircraft Propulsion Systems”. In: (2003), p. 87.

[18] Anthony J Colozza, Analex Corporation, and Brook Park. “Comparison of Mars Aircraft Propulsion Systems”. In: (2003), p. 87.